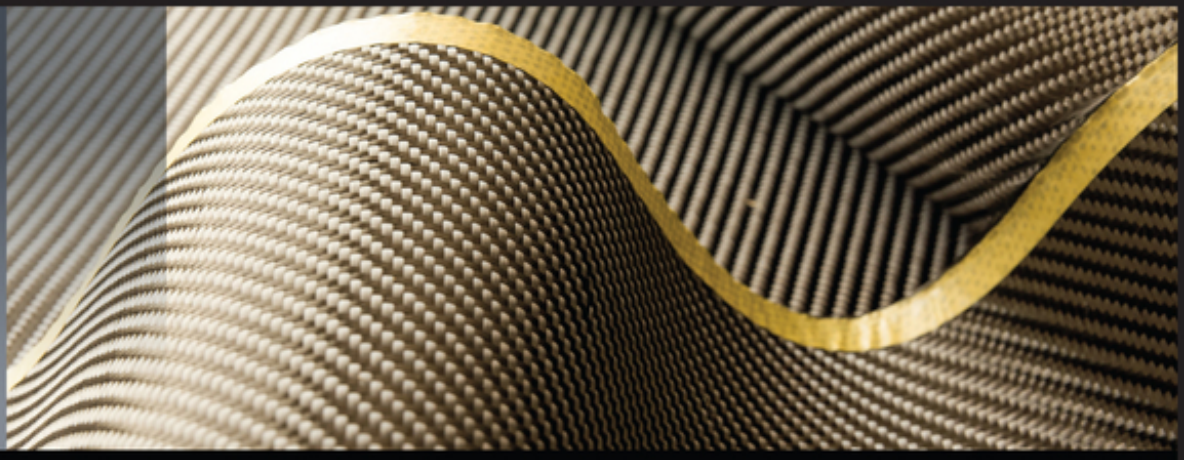

NANOCARBON CHEMISTRY AND INTERFACES

# Novel Carbon Materials and Composites

## Synthesis, Properties and Applications

EDITORS

Xin Jiang
Zhenhui Kang
Xiaoning Guo
Hao Zhuang

WILEY

Novel Carbon Materials and Composites

## Nanocarbon Chemistry and Interfaces

Series Editor
*Nianjun Yang, Institute of Materials Engineering, University of Siegen, Germany*

**Titles in the Series**

Nanocarbons for Electroanalysis
*Sabine Szunerits, Rabah Boukherroub, Alison Downard, Jun-Jie Zhu*

Carbon Nanomaterials for Bioimaging, Bioanalysis and Therapy
*Huan-Cheng Chang, Yuen Yung Hui, Haifeng Dong, Xueji Zhang*

Novel Carbon Materials and Composites: Synthesis, Properties and Applications
*Xin Jiang, Zhenhui Kang, Xiaoning Guo, Hao Zhuang*

**Forthcoming Titles**

Nanocarbon Electrochemistry
*Nianjun Yang, Guohua Zhao, John S. Foord*

Nanocarbons and their Hybrids
*Jean-Charles Arnault, Dominik Eder*

# Novel Carbon Materials and Composites

## Synthesis, Properties and Applications

*Edited by*

*Xin Jiang*
University of Siegen
Germany

*Zhenhui Kang*
Soochow University
People's Republic of China

*Xiaoning Guo*
Institute of Coal Chemistry
Chinese Academy of Sciences
People's Republic of China

*Hao Zhuang*
University of Siegen
Germany

WILEY

This edition first published 2019


*Registered Office*
John Wiley & Sons, Inc., 111 River Street, Hoboken, NJ 07030, USA
John Wiley & Sons Ltd, The Atrium, Southern Gate, Chichester, West Sussex, PO19 8SQ, UK

*Editorial Office*
9600 Garsington Road, Oxford, OX4 2DQ, UK

For details of our global editorial offices, customer services, and more information about Wiley products visit us at www.wiley.com.

Wiley also publishes its books in a variety of electronic formats and by print-on-demand. Some content that appears in standard print versions of this book may not be available in other formats.



*Library of Congress Cataloging-in-Publication Data*

Names: Jiang, Xin, editor. | Kang, Zhenhui, editor. | Guo, Xiaoning, editor. | Zhuang, Hao, editor.
Title: Novel carbon materials and composites : synthesis, properties and applications / edited by Xin Jiang, University of Siegen, Siegen, Germany, Zhenhui Kang, Soochow University, Soochow, People's Republic of China, Xiaoning Guo, Institute of Coal Chemistry, Chinese Academy of Sciences, Taiyuan, Shanxi, People's Republic of China, Hao Zhuang, University of Siegen, Germany.
Description: Hoboken, NJ, USA : Wiley, [2019] | Series: Nancarbon chemistry and interfaces | Includes bibliographical references and index. | Identifiers: LCCN 2018054009 (print) | LCCN 2018057599 (ebook) | ISBN 9781119313601 (Adobe PDF) | ISBN 9781119313618 (ePub) | ISBN 9781119313397 (hardcover)
Subjects: LCSH: Carbon composites.
Classification: LCC TA418.9.C6 (ebook) | LCC TA418.9.C6 N673 2019 (print) | DDC 620.1/93–dc23
LC record available at https://lccn.loc.gov/2018054009

Cover Design: Wiley
Cover Image: © TLaoPhotography/Shutterstock

Set in 10/12pt WarnockPro by SPi Global, Chennai, India

Printed and bound in Spain by Graphycems

10 9 8 7 6 5 4 3 2 1

# Contents

## List of Contributors

***Haiyuan Fu***
Institute of Materials Engineering
University of Siegen
Germany

***Yanfang Gao***
College of Chemical Engineering
Inner Mongolia University of Technology
Hohhot
People's Republic of China

***Xiang-Yun Guo***
State Key Laboratory of Coal Conversion
Institute of Coal Chemistry
Chinese Academy of Sciences
People's Republic of China

and

School of Petrochemical Engineering
Changzhou University
People's Republic of China

***Xiao-Ning Guo***
Institut für Anorganische Chemie, and
Institute for Sustainable Chemistry &
Catalysis with Boron
Julius-Maximilians-Universität Würzburg
Germany

***Yuning Guo***
Institute of Materials Engineering
University of Siegen
Germany

***Hui Huang***
Jiangsu Key Laboratory for Carbon-based
Functional Materials and Devices
Institute of Functional Nano and Soft
Materials (FUNSOM)
Soochow University
People's Republic of China

***Nan Huang***
Shenyang National Laboratory for
Materials Science
Institute of Metal Research
Chinese Academy of Sciences
People's Republic of China

***Xin Jiang***
Shenyang National Laboratory for
Materials Science
Institute of Metal Research
Chinese Academy of Sciences
People's Republic of China

and

Institute of Materials Engineering
University of Siegen
Germany

***Zhenhui Kang***
Jiangsu Key Laboratory for Carbon-based
Functional Materials and Devices
Institute of Functional Nano and Soft
Materials (FUNSOM)
Soochow University
People's Republic of China

***Lijun Li***
College of Chemical Engineering
Inner Mongolia University of Technology
People's Republic of China

***Yang Liu***
Jiangsu Key Laboratory for Carbon-based Functional Materials and Devices
Institute of Functional Nano and Soft Materials (FUNSOM)
Soochow University
People's Republic of China

***Yanhong Liu***
School of Chemistry and Chemical Engineering
Jiangsu University
People's Republic of China

***Baodong Mao***
School of Chemistry and Chemical Engineering
Jiangsu University
People's Republic of China

***Weidong Shi***
School of Chemistry and Chemical Engineering
Jiangsu University
People's Republic of China

***Zijun Shi***
College of Chemical Engineering
Inner Mongolia University of Technology
People's Republic of China

***Qingquan Tian***
Shenyang National Laboratory for Materials Science
Institute of Metal Research
Chinese Academy of Sciences
People's Republic of China

***Xi-Li Tong***
State Key Laboratory of Coal Conversion
Institute of Coal Chemistry, Chinese Academy of Sciences
People's Republic of China

***Nianjun Yang***
Institute of Materials Engineering
University of Siegen
Germany

***Zhaofeng Zhai***
Shenyang National Laboratory for Materials Science
Institute of Metal Research
Chinese Academy of Sciences
People's Republic of China

***Hao Zhuang***
Institute of Materials Engineering
University of Siegen
Germany

## Series Preface

Carbon, the sixth element in the Periodic Table, is extraordinary. It forms a variety of materials because of its ability to bond covalently with different orbital hybridizations. For millennia, there were only two known substances of pure carbon atoms: graphite and diamond. In the mid-1980s, a soccer-ball-shaped buckminsterfullerene, namely a new carbon allotrope C60, was discovered. Together with other fullerene-structures (C70, C84), the nanocarbon researcher was spawned. In the early 1990s, carbon nanotubes were discovered. They are direct descendants of fullerenes, and capped structures composed of 5- and 6-membered rings. This was the next major advance in nanocarbon research. Due to their groundbreaking work on these fullerene materials, Curl, Kroto and Smalley were awarded the 1996 Nobel Prize in Chemistry. In the beginning of the 2000s, graphene was prepared using Scotch tape. It is a single sheet of carbon atoms packed into a hexagonal lattice with a bond distance of 0.142 nm. For their seminal work with this new nanocarbon material, Geim and Novoselov were awarded the 2010 Nobel Prize in Physics. New members, carbon nanoparticles, such as diamond nanoparticles, carbon dots, and graphene (quantum) dots, have emerged in the family of nanocarbon materials. Although all these materials only consist of the same carbon atoms, their physical, chemical, and engineering features are different, and fully dependent on their structures and surface functional groups.

The purpose of this series is to bring together up-to-date accounts of recent developments and new findings in the field of nanocarbon chemistry and interfaces, one of the most important aspects of nanocarbon research. The carbon materials covered in this series include diamond, diamond nanoparticles, graphene, graphene-oxide, graphene (quantum) dots, carbon nanotubes, carbon fibers, fullerenes, carbon dots, carbon composites, and their hybrids. The formation, structure, properties, and applications of these carbon materials are summarized. Their relevant applications in the fields of electroanalysis, biosensing, catalysis, electrosynthesis, energy storage and conversion, environment sensing and protection, biology and medicine are highlighted in different books.

I wish to express my sincere thanks to Miss Sarah Higginbotham, Jenny Cossham, Emma Strickland, and Lesley Jebaraj from Wiley's Oxford office. Without their efficient help and valuable suggestions during this project, the publication of this book series would not be possible. Last, but not least, I want to thank my family, especially my

wife, Dr Xiaoxia Wang, and my children Zimo and Chuqian Luisa, for their constant and strong support as well as for their patience in letting me finalize such a book series.

February 2017

*Nianjun Yang*
*Siegen, Germany*

# Preface

Novel carbons and carbon-related films are newly developed functional materials. Among them, carbon dots, silicon carbide, and carbon nitrides have been paid most attention. In recent years, the fabrication of novel carbon composites is also becoming a hot research topic because these composites address certain disadvantages of novel carbon materials, and further extend their potential applications. The synthesis, properties, and applications of novel carbon composites, such as diamond/SiC composites and diamond/graphite composites, have been widely reported and discussed. The object of this book is to provide an excellent entry into recent progress and achievements in these subjects, centered on novel carbon materials and their composites.

This book consists of two parts. In the first part, the synthesis, properties and applications of novel carbon materials, including silicon carbide, carbon nitrides, and nanocarbons are reviewed. Chapters 1 and 2 concentrate on silicon carbide films, where chemical vapor deposition of silicon carbide films and their electrochemical applications are presented. Chapter 3 is about synthesis and photocatalytic applications of silicon carbide powders featuring high surface areas. Chapter 4 discusses the fabrication of graphite carbon nitrides, summarizes their bandgap and nanostructure engineering, and highlights their water splitting applications. The applications of various novel carbon materials for the construction of supercapacitors are shown in Chapter 5.

The synthesis, properties and applications of novel carbon composites are summarized in the second part of this book. In Chapter 6, chemical vapor deposition of diamond/silicon carbide composite films is detailed, including applied instruments, conditions, properties, and growth mechanisms. Their mechanical, sensing, and biochemical applications are shown. Chapter 7 describes the related contents for diamond/graphite composite films. Their electrochemical applications are highlighted. In the last chapter of this book, carbon nanodot composites are shown, covering their fabrication processes and properties, and highlighting their use in catalytic applications, sensing and detection, environment, energy storage and conversion.

From our point of view, this book presents hot topics taking into account recent progress and achievements in the fields of novel carbon materials and composites. It is hoped that this book stimulates graduate students and young scientists, as well as experienced researchers, to explore these novel carbon materials and composites in their fundamental and practical aspects in future.

Finally, we thank all the scientists who contributed chapters to this book, as well as colleagues from Wiley who kindly devoted their time and efforts to allow this book to be smoothly published.

*Xin Jiang*
*Siegen, Germany*

*Zhenhui Kang*
*Suzhou, People's Republic of China*

*Xiaoning Guo*
*Taiyuan, People's Republic of China*

*Hao Zhuang*
*Siegen, Germany*

# 1

# Cubic Silicon Carbide: Growth, Properties, and Electrochemical Applications

*Nianjun Yang and Xin Jiang*

*Institute of Materials Engineering, University of Siegen, Paul-Bonatz-Str. 9-11, 57076 Siegen, Germany*

## 1.1 General Overview of Silicon Carbide

It is well known that carbon and silicon atoms form similar, covalently bonded and giant structures, as shown schematically in Figure 1.1a. They are thus called carbon diamond and silicon diamond. In both diamond structures, each atom is covalently bonded to four other atoms located at the corner of a tetrahedron. Another diamond-like compound is silicon carbide (SiC), building up with silicon and carbon atoms. In this crystal, each atom is $sp^3$-hybridized and forms four bonds to four other atoms of the opposite kind. The tetrahedral arrangement of atoms encountered in the pure carbon and silicon diamond structures is preserved in SiC (Figure 1.1a).

The existence of a compound containing SiC bonds was proposed in 1824 for the first time by Jöns Jacob Berzelius, a Swedish chemist [1]. In 1905, Henri Moissan, a French chemist and the Nobel laureate, discovered SiC in nature [2]. In mineralogy, SiC is therefore known as moissanite [3]. In nature, moissanite SiC is very rare and only found in certain types of meteorite. The most commonly encountered SiC material is actually man-made.

SiC exists in about 250 crystalline forms, as variations of the same chemical compound that are identical in two dimensions but differ in the third. They can be viewed as layers stacked in a certain sequence. Different stacking sequences of C-Si double layers lead to different crystalline structures, or so-called polytypes [4]. Therefore, more than 250 polytypes have been predicted [4, 5]. Of these polytypes, only a few of them have been studied in detail. In principle, only three are of major importance: cubic (3C, or β)-SiC, 4H-SiC, and 6H(α)-SiC, which are shown schematically in Figure 1.1b–d, respectively. The most commonly encountered polymorph is 6H(α)-SiC, which forms at temperatures higher than 1700°C and has a hexagonal crystal structure (similar to wurtzite) (Figure 1.1c). Cubic 3C(β)-SiC (Figure 1. 1b) is formed at temperatures below 1700°C and has a zincblende (ZnS) crystal structure, similar to diamond [6].

### 1.1.1 SiC Properties

SiC is a fascinating material, although it has quite complicated polytypes. This is because the type of SiC polytype implies a corresponding set of relevant physical properties.

*Novel Carbon Materials and Composites: Synthesis, Properties and Applications,* First Edition.
Edited by Xin Jiang, Zhenhui Kang, Xiaoning Guo and Hao Zhuang.

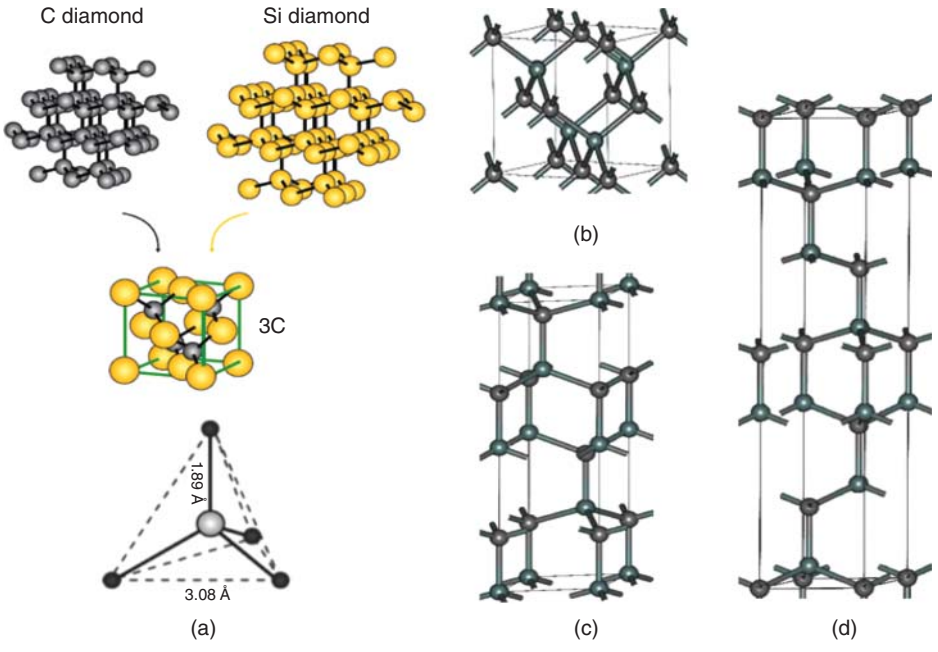


**Figure 1.1** Chemical structures of carbon diamond, silicon diamond, SiC (a), 3C(β)-SiC (b), 4H-SiC (c), and 6H(α)-SiC (d) using ball-stick models.

As examples, some important physical properties of 4H-, 6H-, and 3C-SiC are listed in Table 1.1, compared with those of diamond and silicon.

SiC has been known for decades to be a semiconductor, based on the very first electroluminescence (yellowish light) from SiC crystals when subjected to electricity in 1907 [7]. More interestingly, its indirect bandgap is tunable in the range of 2.36–3.23 eV, determined by the polytype of SiC films. For instance, the bandgaps for 3C-, 4H-, and 6H-SiC are 2.36, 3.23, and 3.05 eV, respectively. However, SiC can be varied from insulating, semiconductive, to metallic-like in its properties when the dopants (n- or p-type) and the doping levels are altered. For example, SiC films can be doped with either n-type dopants (e.g. nitrogen, phosphorus) or p-type dopants (e.g. beryllium, boron, aluminum, gallium). Metallic conductivities of SiC films have been achieved by their heavy doping with boron, aluminum, or nitrogen. For example, at the same temperature of 1.5 K, superconductivity has been detected in 3C-SiC films doped with aluminum and boron as well as in 6H-SiC films doped with boron.

In comparison with Si, SiC has a higher thermal conductivity, electric field breakdown strength, and current density. It features a very low coefficient of thermal expansion ($4.0 \times 10^{-6}$ $K^{-1}$) and experiences no phase transitions that cause discontinuities in thermal expansion. The sublimation temperature of SiC is very high (approximately 2700°C), which makes it useful for bearings and furnace parts. SiC does not melt at any known temperature.

SiC is transparent to visible light. Pure SiC is colorless. The brown to black color of industrial SiC products results from iron impurities. The rainbow-like lusters of SiC crystals are caused by the passivation layers of $SiO_2$ that form on the SiC surface.

**Table 1.1** Basic properties of three kinds of SiC, Si, and diamond.

| Property | 4H-SiC | 6H-SiC | 3C-SiC | Si | Diamond |
|---|---|---|---|---|---|
| Energy bandgap at 300 K (eV) | 3.20 | 3.00 | 2.29 | 1.12 | 5.45 |
| Intrinsic carrier concentration at 300 K ($cm^{-3}$) | $5 \times 10^{-9}$ | $1.6 \times 10^{-6}$ | $1.5 \times 10^{-1}$ | $1 \times 10^{10}$ | $\sim 10^{-27}$ |
| Critical breakdown electric field (MV $cm^{-1}$) | 2.2 | 2.5 | 2.12 | 0.25 | 1–10 |
| Saturated electron drift velocity ($\times 10^7$ cm $s^{-1}$) | 2.0 | 2.0 | 2.5 | 1.0 | 1.5 |
| Electron mobility ($cm^2$ $V^{-1}$ $s^{-1}$) | 1000 | 600 | 800 | 1450 | 480 |
| Electron mobility ($cm^2$ $V^{-1}$ $s^{-1}$) | 115 | 100 | 40 | 470 | 1600 |
| Thermal conductivity at 300 K (W $cm^{-1}$ $K^{-1}$) | 3.7 | 3.6 | 3.6 | 1.49 | 6–20 |
| Coefficient of thermal expansion at 300 K ($10^{-6}$ $K^{-1}$) | 4.3<br>4.7 | 4.3<br>4.7 | 3.2 | 3.0 | 1.0 |
| Lattice coefficient (a, c in Å) | a = 3.073<br>c = 10.053 | a = 3.081<br>c = 15.117 | a = 4.360 | a = 5.430 | a = 3.567 |
| Calculated elastic coefficient (GPa) | $C_{44} = 600$ | $C_{11} = 500$<br>$C_{12} = 92$<br>$C_{44} = 168$ | $C_{11} = 352$<br>$C_{12} = 12$<br>$C_{44} = 233$ | $C_{11} = 167$<br>$C_{12} = 65$<br>$C_{44} = 80$ | $C_{11} = 1079$<br>$C_{12} = 124$<br>$C_{44} = 578$ |

SiC is a very hard material. Taking Mohs hardness scale as an example, the value of talc is given by 1 and diamond is given by 10: SiC has the value of 9.3 [8].

SiC is chemically inert. For example, it is resistive to radiation and many chemicals. This is because the electron bonds between the silicon and carbon atoms inside SiC are extremely strong. More importantly, SiC has shown superior biocompatibility and is non-toxic in both *in vitro* and *in vivo* tests. In addition, SiC is multifunctional, originating from the possibility of adopting both silicon and carbon chemistry on its surface.

In conclusion, SiC is a material with exceptional physical properties (e.g. a low density, a high strength, a high thermal conductivity, high stability at high temperatures, a high resistance to shocks, low thermal expansion, a high refractive index, a wide but tunable bandgap) and chemical features. They present multiple options for smart devices through their electrical, chemical, and optical properties [5, 9–15].

### 1.1.2 SiC Applications

Thanks to its unique physical properties (e.g. electrical, thermal properties), SiC has found wide and varied applications where high blocking voltages or high switching frequencies are required [5, 9–15]. Shockley thus predicted in the 1950s that SiC would quickly replace Si. SiC-based power electronics can greatly reduce the power losses of electrical energy in most generators and distribution systems. The higher frequency,

smaller dimensions, reduced cooling requirements, and greater efficiency obtained with SiC power electronics will give more efficient systems in any application where AC-DC, DC-AC, or DC-DC conversion is required. One example application of SiC is for compact power supply units with extremely low losses, which also keep the power supply network free of electric smog (the unwanted interference frequencies resulting from the use of computers) [5, 15].

SiC is also suited for space-saving control units and for variable-speed drives, which are generally mounted directly on the mortars. For these applications, homoepitaxial SiC films are generally required. However, the typical growth rate for homoepitaxial SiC layers is 5–10 μm $h^{-1}$. Thus, the epitaxial growth of SiC layers is very time-consuming, making them very expensive for most devices. The long production time and high cost of these epitaxial SiC layers are thus the main obstacles to overcome, in order to make SiC power devices more available to market [5, 11, 15]. In contrast, the latest discovery of new forms of SiC (e.g. nanoporous structures, superlattices) has triggered the development of SiC electronics, and in particular thin-film technologies [11].

Bulk SiC has become a more important compound in materials science, such as a support for loading heterogeneous catalysts, for hard coating (e.g. for cutting), for implantable sensors, and for protein separation and micro-fluidic systems where a porous SiC film is needed. Especially in recent years there has been increased attention to employing SiC as a valuable material for biomedical applications and as a transducer for biosensors. This is because SiC has the advantages of its chemical, tribological, and electrical properties. In addition, it can easily be integrated on a chip into a system. For example, SiC has been employed as an active material for micro-device fabrication [13, 14]. In addition, SiC offers an ideal surface to grow graphene, another important material with superior physical, chemical and electrical properties [16].

### 1.1.3 Scope of this Chapter

Since the physical and mechanical properties of SiC films and their related nanostructures (e.g. particles, wires, pores, etc.) as well as their applications in the fields of electronics, power devices, and biomedical applications have been widely reviewed and discussed [5, 9–15], we focus in this chapter only on the growth, interfacial properties, and electrochemical applications of 3C-SiC. The growth of 3C-SiC using various chemical vapor deposition (CVD) techniques is summarized. After the description of the interfacial properties (e.g. surface morphology, surface chemistry, and electrochemical properties) of 3C-SiC, the electrochemical applications of 3C-SiC films in the fields of electrochemical and biochemical sensing, energy storage and conversion are highlighted. Finally, we close this chapter with concluding remarks as well as discussion about the future research directions of 3C-SiC.

## 1.2 Synthesis of Silicon Carbide

### 1.2.1 Acheson Process

SiC is traditionally produced through the so-called Acheson process, where an Acheson graphite electric resistance furnace is required. At very high temperatures (>2500°C), a solid-state reaction occurs between two precursors, namely silica sand and petroleum coke, leading to the formation of SiC [15]. Crystalline SiC synthesized by the Acheson

process features different polytypes and varies in its purity. The common impurities are nitrogen and aluminum. By altering the heating processes and/or the distances of the graphite resistor heat source of the Acheson furnace, colorless, transparent, or variously color SiC films have been synthesized [17]. These manufactured SiC films have large grain sizes and are invariably contaminated with oxygen. Such an Acheson process is still used for the production of polycrystalline SiC films, which are often known by the name carborundum. The as-obtained SiC ceramic is quite suitable for grinding and cutting applications, such as abrasive and cutting tools. However, the Acheson process requires excessive energy input during SiC synthesis, and the quality of the synthesized SiC is rather poor.

### 1.2.2 Physical Vapor Transport

Several alternative methods have since been developed for the synthesis of pure SiC films. Physical vapor transport (PVT) is the most popular and successful method for growing large single SiC crystals [18, 19]. As the first method of the sublimation technique (also known as the Lely method) [20], the synthesis of SiC with limited crystal sizes was carried out under argon ambient at about 2500°C in a graphite container. The formed SiC crystals (or Lely platelets) presented good quality (e.g. micropipe densities of 1–3 $cm^{-2}$, dislocation densities of $10^2$–$10^3$ $cm^{-2}$). Unfortunately, this technique has several major shortcomings, such as uncontrollable nucleation rates and dendrite-like growth processes. Later, a modified PVT method (also called the modified-Lelly method or seed sublimation method) was proposed. Such a method controlled SiC growth and improved the limited adjustment of the gas phase composition between the concentrations of dopant species and the complements of C and Si [21]. The sources and the seeds of SiC were placed perfectly in close proximity to each other, where a gradient of temperatures was established. In such a way, the transport of the material vapor above the seeds became possible at a low argon pressure. The conventional PVT method was further refined through a gas pipe between the source and the crucible into the growth chamber (M-PVT setup) [22, 23]. By use of such a M-PVT setup, high-quality 4H- and 6H-SiC wafers have been grown, with diameters up to 100 mm. An additional gas pipe was used to introduce dopant gases and/or small amounts of C- and Si-bearing gases ($SiH_4 : H_2 = 1 : 10$, propane). Namely, the gas phase composition was further controlled. By use of such a modified M-PVT setup, 15R-SiC and 3C-SiC have been also synthesized [23].

### 1.2.3 Chemical Vapor Deposition

The CVD technique is another suitable and widely investigated method to produce SiC samples in various forms (e.g. thin films, powders, whiskers, and nanorods, etc.) [16, 24–57]. For example, amorphous SiC powders have been prepared by a CVD method, where $SiH_4$ and $C_2H_2$ acted as the precursors and nitrogen as the carrying gas [24, 25].

Atmospheric pressure chemical vapor deposition (APCVD) is one of the first CVD techniques developed to deposit SiC [25]. During deposition, a carbonization process is initially applied to a clean Si surface, followed by SiC growth using Si- and C-containing precursors [26–28]. SiC growth rates of up to several $\mu m\, h^{-1}$ have been achieved, with the potential to be doped into n- and p- type materials. An APCVD system is a relatively

simple and easy setup due to the incorporation of few temperature sensitive components. Both epitaxial and polycrystalline 3C-SiC films have been deposited by APCVD. It is particularly advantageous for SiC epitaxy, where higher temperatures (1300°C) are typically required for the growth of single crystals of SiC on Si substrates.

Low-pressure chemical vapor deposition (LPCVD) is the second CVD system utilized for the growth of SiC films. Although the growth rates of SiC films during LPCVD processes are much lower than those in APCVD processes, generally more substrates can be accommodated in LPCVD systems, especially when resistive heating is used. Due to the vacuum system involved for a LPCVD system, it has much lower chamber pressure in comparison with an APCVD system. Therefore, a LPCVD reactor allows the exploitation of more varieties of precursors, as well as reducing impurity incorporation in the deposited films. In short, the LPCVD process generates generally higher quality SiC films with much better uniformity across large substrate areas. By means of LPCVD techniques, epitaxial 3C-SiC films have been grown on Si wafers [29]. In recent years, LPCVD has actually become a leading technique for the growth of polycrystalline 3C-SiC films on various substrates including $SiO_2$ and $Si_3N_4$. Doping can also be achieved during LPCVD processes, conducted by simply adding dopants (e.g. 1,3-disilabutane, nitrogen, etc.) into the feed gases [30–35]. For example, controlled nitrogen doping has been demonstrated by adding nitrogen or $NH_3$ as the precursor into the feed gases. By varying the fractions of dichlorosilane and 1,3-disilabutane in the gas mixtures, the residual stress and strain gradient of polycrystalline SiC films has been tuned [36].

The third CVD technique applied for the synthesis of SiC films is metal organic chemical vapor deposition (MOCVD), which is especially useful for the growth of thick SiC films on sapphire (001) and silicon (111) substrates. Diethylmethylsilane (DEMS) containing both Si and C atoms was used as an individual precursor. No gas carrier or bubbler was thus applied. The films grown at low temperatures (850 and 900°C) on both substrates showed crystalline 3C-SiC in the (111) orientation [37].

Plasma enhanced chemical vapor deposition (PECVD) has been employed to deposit SiC films at low temperatures. Due to the use of low temperatures during PECVD processes, it is feasible to deposit SiC on a variety of materials (e.g. aluminum) that are not possible during APCVD and LPCVD processes. Commercially available PECVD systems can thus be utilized for processes that benefit from future mass production of SiC. The low deposition temperatures also confirm its potential suitability for related processing. To grow SiC by means of PECVD, gas precursors such as $SiH_4$ and $CH_4$ [38, 39] as well as liquid sources such as $C_6H1_8Si_2$ (hexamethyldisilane) [40] have been used. The as-deposited SiC films are amorphous, and thus post-deposition annealing is required for crystallization. Altering deposition parameters such as pressure and gas flow ratios resulted in the control of the stress in the deposited films during these PECVD processes [39]. Moreover, both doped and undoped SiC can be synthesized by PECVD [41–47]. We have employed microwave plasma chemical vapor deposition (MWCVD) techniques to grow three different kinds of 3C-SiC films, namely nanocrystalline, microcrystalline and epitaxial (001) 3C-SiC films [16]. Table 1.2 lists the depositional conditions we applied for the growth of these 3C-SiC films by means of MWCVD.

Figure 1.2 shows scanning electron microscopy (SEM) and atomic force microscopy (AFM) images of three 3C-SiC films [16]. The nanocrystalline 3C-SiC film possesses a crystal size smaller than 50 nm (Figure 1.2a). Its surface is relatively smooth and

**Table 1.2** Depositional parameters for the MWCVD growth of three 3C-SiC films [16].

| Film type | Microwave power (W) | Gas pressure (Torr) | $T_s$ (°C) | TMS content (ppm) |
|---|---|---|---|---|
| Nanocrystalline | 700 | 20 | ~800 | 290 |
| Microcrystalline | 1800 | 45 | ~700 | 290 |
| Epitaxial | 2200 | 55 | ~850 | 140 |

Source: Reprinted with permission from ACS publisher.

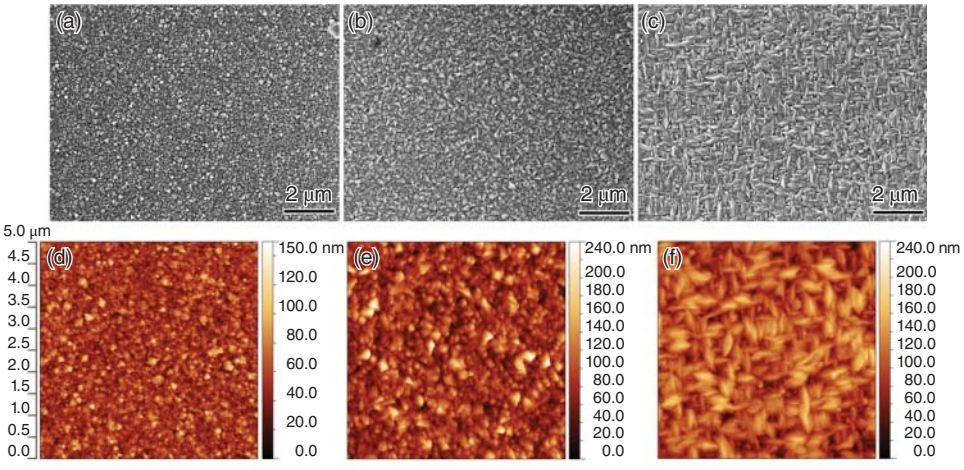


**Figure 1.2** SEM (a–c) and AFM non-contact mode (d–f) images of a nanocrystalline (a, d), a microcrystalline (b, e), and an epitaxial (c, f) 3C-SiC film. The sizes of the AFM images are $5 \times 5\ \mu m^2$ [16]. Source: Reprinted with permission from ACS publisher, Copyright 2015.

has a root-mean-square (RMS) roughness of only 12.6 nm, as estimated from its AFM non-contact mode image shown in Figure 1.2d. The average crystal size of the microcrystalline 3C-SiC film is ~200 nm (Figure 1.2b). Its larger crystal size results in its higher surface roughness, which is measured to be 22.9 nm from the AFM image (Figure 1.2e). The SEM image of the epitaxial 3C-SiC film (Figure 1.2c) shows densely packed 3C-SiC crystals lying along the {110} directions of the Si wafer, presenting the very typical nature of heteroepitaxially grown 3C-SiC crystals on (001) Si [16, 48]. Its surface roughness is comparable to that of the microcrystalline 3C-SiC film, which is 20.6 nm determined by the AFM measurement (Figure 1.2f).

Remote microwave hydrogen plasma chemical vapor deposition (RPCVD) has been applied to grow amorphous hydrogenated SiC (a-SiC : H) films. Dimethylsilane (DMS) or tetramethylsilane (TMS) was used as a single-source precursor [49]. The Arrhenius plots of substrate temperature dependencies of the thickness-based film growth rate implied that the investigated RPCVD for DMS precursor is a non-thermally activated process, whereas for TMS precursor it is an adsorption-controlled one. An increase in the substrate temperature from 30 to 400°C caused the elimination of organic moieties from the films and the formation of SiC networks. These a-SiC : H films proved to be

useful as scratch-resistant protective coatings for optical glass elements and various metal surfaces [49].

Some other CVD techniques have been employed to grow 3C-SiC films. For example, the halide CVD process was applied to fabricate oriented stoichiometric 3C-SiC films in a rapid way. During such a process, the flow rates of precursors ($SiCl_4$ and $CH_4$) were controlled [54]. The (110)-oriented stoichiometric 3C-SiC films with lower densities of defects were obtained when the molar ratios of C precursor to Si precursor were in the range of 0.86–1.00. The maximum deposition rate was 883 μm $h^{-1}$ when the molar ratio of C precursor to Si precursor reached 1.00, leading to a thickness of 1.7 mm in a deposition time of two hours. A twin plane propagation model has been proposed to explain the formation of ridge-like morphologies of SiC films. Another example, the low pressure hot-wall CVD technique, has been used for the growth of 3C-SiC films on Si (100) substrates [55]. The C/Si ratio played an important role in the crystalline quality and surface morphology of 3C-SiC films. Comparisons indicate that the optimal C/Si ratio for high crystalline quality of 3C-SiC films is 4.5. Noticeably, the polycrystalline grains of 3C-SiC films exhibited an epitaxial nature with irregular shapes and random distribution. Pyramid-like shapes and regular distribution were found along the {110} directions, dependent on the C/Si ratios. The changes in crystalline quality with increasing C/Si ratios were attributed to the competition of the formation of defects by excess carbon species with the etching of the atomic hydrogen. Meanwhile, the changes of surface morphology were due to the changes in secondary nucleation rates.

In past decades, more efforts have contributed to achieving homoepitaxial CVD growth of 3C-SiC films. Typically, it was done using silane ($SiH_4$) as the silicon precursor, and light hydrocarbons (e.g. ethylene or propane) as the carbon precursor. In some cases, only TMS was used as the precursor. Hydrogen gas, sometimes mixed with some argon, was used as carrier gas. The growth temperature and pressure were usually between 1500 and 1650°C and 100–1000 mbar, respectively. For example, the laser CVD technique has been applied for the epitaxial growth of 3C-SiC thin films on Si(001) substrates [50]. The epitaxial relationship was 3C-SiC(001){111}//Si(001){111} and multiple twins {111} planes were identified. The maximum deposition rate was 23.6 μm $h^{-1}$, which is about 5–200 times higher than that of conventional CVD methods. The density of twins increased with an increase in the thickness of 3C-SiC films. The cross-section of the films exhibited a columnar structure, containing twins at {111} planes that were angled at 15.8° to the surface of Si(001) substrates [50].

Conventional CVD equipment (c-CVD) was also employed for the growth of epi-SiC/Si-wafer/epi-SiC [51]. The Si wafer was double-side polished and mounted with a suspension mode in the c-CVD chamber. Homogeneous 3C-SiC (100) films were heteroepitaxially grown simultaneously on both surfaces of the suspended Si (100) wafer. Each film was uniform and continuous, with same trend of slight degradation from the inner to the outer region of the wafer. This technique offered a possible way to mass-produce high-quality 3C-SiC films on Si wafers in one run. The potential applications of 3C-SiC films (e.g. sensors, etc.) were thus also expanded.

Using PECVD techniques, the epitaxial deposition of 3C-SiC films has been achieved on (100) Si substrates [52]. A high density of defects (e.g. misfit dislocations, stacking faults, and twin boundaries) was generated in the film. Defect-induced strain distribution in the 3C-SiC film was analyzed by the geometric phase analysis method combined with X-ray diffraction (XRD) and Raman spectroscopy. The strain analysis at an atomic level revealed that periodic misfit dislocations at the interface generate high local

compressive strain (>20%) around the core of the dislocations in the SiC film, relaxing a major part of the intrinsic strain. A highly compressive interfacial layer was found to form between the SiC film and Si substrate, regardless of the carbonization temperature. This interfacial layer was linked with the carbonization step of the film growth process. In addition, twins and stacking faults provided a complementary route for strain relaxation during the film growth process. More strain was accommodated at the matrix/twin interface during twin nucleation rather than that at the growth stage.

The controlled growth of heteroepitaxial 3C-SiC films was achieved by use of a 915 MHz MWCVD reactor [53]. TMS and hydrogen were used as the resource gases. With an increase in MW power, the morphology of the SiC crystals evolved from randomly oriented nanocrystals to well-oriented pyramid-shaped crystals. Suggested from the rocking curves, the 3C-SiC film deposited at a MW power of 9 kW and a gas pressure of 50 mbar remained epitaxial in nature. An increase in TMS gas flow rates did not affect such an epitaxial feature. Uniform heteroepitaxial deposition of 3C-SiC film on 4-in. silicon wafer was then realized at a low deposition temperature (~860°C).

Various SiC nanostructures have been grown using CVD techniques [56, 57]. For example, the morphology control of one-dimensional (1D) SiC nanostructures was achieved by manipulating the composition of the catalysts (e.g. $Fe_5Si_3$, $Fe_3Si$) during MWCVD processes. Iron silicide was found to be the main catalyst to initiate the growth of 1D SiC nanostructures. As confirmed by high-resolution transmission electron microscopy (HRTEM), the stoichiometry of iron silicide governed the final morphology of 1D SiC nanowires (NWs). For the growth of SiC NWs, the catalyst is $Fe_5Si_3$, while it is $Fe_3Si$ for the growth of SiC nanoneedles. A special orientation match between iron silicide catalyst and SiC NWs was observed during the growth of 1D SiC nanostructures, due to different etching resistivities of the catalyst particles under $H_2$ plasma [56]. Direct synthesis of ordered 3C-SiC nanosheet arrays has been also realized in a MWCVD reactor through utilizing planar defects formed during hetero-epitaxial growth of crystals with close-packed lattices [57]. TMS was used as a single source precursor and diluted in hydrogen gas. The plasma with a high MW power (e.g. 2500 W) was applied to activate the gas phase reaction. With a very low concentration of TMS (e.g. 140 ppm), the growth of the 3C-SiC epitaxial layer was achieved at a low growth rate (~50 nm $h^{-1}$). The grown 3C-SiC nanosheet arrays are well oriented on (001) and (111) Si substrates. The planar defects and the plasma environment were identified as key factors to determine the resulting 2D nanosheet arrays. Consequently, a "planar defect induced selective growth" effect was proposed to elucidate the corresponding growth mechanism [57].

In summary, various 3C-SiC films and nanostructures have been grown at different sizes (>3 in.) by altering CVD techniques, substrates, and growth parameters (e.g. power density, gas pressure, type and concentration of precursors, and growth temperature, etc.).

## 1.3 Properties of Cubic Silicon Carbide

### 1.3.1 Surface Morphology

From further analysis of growth conditions summarized in Table 1.2, one can see that the changes in morphology of three 3C-SiC films are possible by controlling the MW

powers, gas pressures, and the concentrations of TMS precursors during MWCVD deposition [52]. For example, at low MW powers and high TMS concentrations, nanocrystalline 3C-SiC films are grown. This is because of high secondary nucleation rates under these conditions. An increase in the MW power enhances the concentration of atomic hydrogen, which is an important species in determining the crystallinity of a 3C-SiC film during MWCVD deposition [52, 58]. It removes the defects and amorphous phase in a 3C-SiC film through a continuous etching process [52, 58]. The higher the concentration of atomic hydrogen, the stronger the etching will be. Since the defects and amorphous phase can serve as sites for secondary nucleation, their effective removal will improve in turn the crystallinity of the 3C-SiC films [52, 58]. As a result, microcrystalline 3C-SiC films with larger crystal sizes and higher crystal quality are formed at high MW powers. Further increase in MW power or reduction of TMS concentrations led to the epitaxial growth of 3C-SiC films on the (001) Si wafer [52].

More detailed information about the composition of nanocrystalline, microcrystalline, and epitaxial 3C-SiC films has been revealed by XRD measurements. Peaks positioning at 35.6°, 41.4°, 60.0°, and 90.0° are indexed to the (111), (200), (220), and (400) reflexes of 3C-SiC, respectively. However, certain differences are observable. For both nanocrystalline and microcrystalline 3C-SiC films, strong (111) reflex exists. Weak (220) reflex is only observed for the microcrystalline 3C-SiC film: an indication of its polycrystalline nature. The intensity of the (220) reflex is much weaker in the nanocrystalline 3C-SiC film. For the epitaxial 3C-SiC film, only (200) and (400) reflexes are present, indicating its perfect (001) orientation [16].

Except for the 3C-SiC crystals, it is well understood that amorphous phases normally form at the grain boundaries during the CVD growth of 3C-SiC films [52]. Such information for these three 3C-SiC films was confirmed using micro-Raman measurements [16]. For all 3C-SiC films, the characteristic Raman peak at ~800 $cm^{-1}$ is observable, corresponding to the transverse optical (TO) phonon of SiC. The full width at half maximum (FWHM) of this SiC TO peak for nanocrystalline, microcrystalline, and epitaxial 3C-SiC films is >40, 17, and 24 $cm^{-1}$, respectively. In comparison with that for a nanocrystalline 3C-SiC film, the SiC TO peaks for both microcrystalline and epitaxial 3C-SiC films are sharper, indicating their better crystallinity. In addition to the SiC TO band, peaks corresponding to the existence of an amorphous carbon phase are also observable at ~1320 $cm^{-1}$ (D band) and ~1600 $cm^{-1}$ (G band) for both nanocrystalline and microcrystalline 3C-SiC films. Nevertheless, since the Raman efficiency of SiC is only a tenth of that of the amorphous carbon [59], the strong D and G bands do not imply an extremely large amount of amorphous carbon phase in the 3C-SiC films. A broad peak positioning at ~900 $cm^{-1}$ is attributed to the Si-C rocking in Si-$CH_3$ [60–63]. The existence of the C-H bonding has been further confirmed by the secondary ion mass spectrometry (SIMS) measurements [64]. Such an observation indicates the presence of the amorphous SiC phase in both 3C-SiC films [60–63]. However, these three peaks completely disappear in the epitaxial 3C-SiC film. This result indicates strongly that no amorphous phase is incorporated into the epitaxial 3C-SiC film. In other words, the epitaxial 3C-SiC film is composed solely of 3C-SiC crystal. Furthermore, a shift in the position of this SiC TO peak is observed. For the microcrystalline and nanocrystalline 3C-SiC films, it shifts to lower wavenumbers in comparison with that of the epitaxial 3C-SiC film, indicating reduced crystallinity for both microcrystalline and nanocrystalline 3C-SiC films. However, a slight upshift

of this SiC TO peak for a nanocrystalline SiC film in comparison with that of a microcrystalline SiC film is reasonable. This is because the nanocrystalline 3C-SiC film contains more amorphous phase, whose thermal expansion coefficient is different from that of a microcrystalline 3C-SiC film. Moreover, the thickness of the nanocrystalline 3C-SiC film is different from that of the microcrystalline 3C-SiC film. These factors lead to the different stress levels in the nanocrystalline 3C-SiC film, resulting in the upshift of its Raman peak in comparison with that of the microcrystalline 3C-SiC film.

To get deep insight into the microscopic structures of nanocrystalline, microcrystalline, and epitaxial 3C-SiC films, their transmission electron microscopy (TEM) images were recorded. As shown in Figure 1.3, the difference in crystal sizes of these 3C-SiC films is clearly seen even from their low magnification TEM images. For the nanocrystalline 3C-SiC film, two kinds of crystals are present but with significant difference in their sizes, as indicated in Figure 1.3a with arrows. The small crystals are about ~5 nm in size, whereas the large ones are tens of nanometers in size. They were confirmed to be 3C-SiC crystals by HRTEM measurements. As shown in Figure 1.3d, the typical lattice fringes of these 3C-SiC crystals feature an interplanar spacing of 0.252 nm for their {111} planes. Moreover, a certain amount of planar defects (twins and stacking faults) is found in these crystals. Those twins and stacking faults lie parallel to the {111} planes, as denoted by the circles in Figure 1.3d. Regardless of their higher crystallinity,

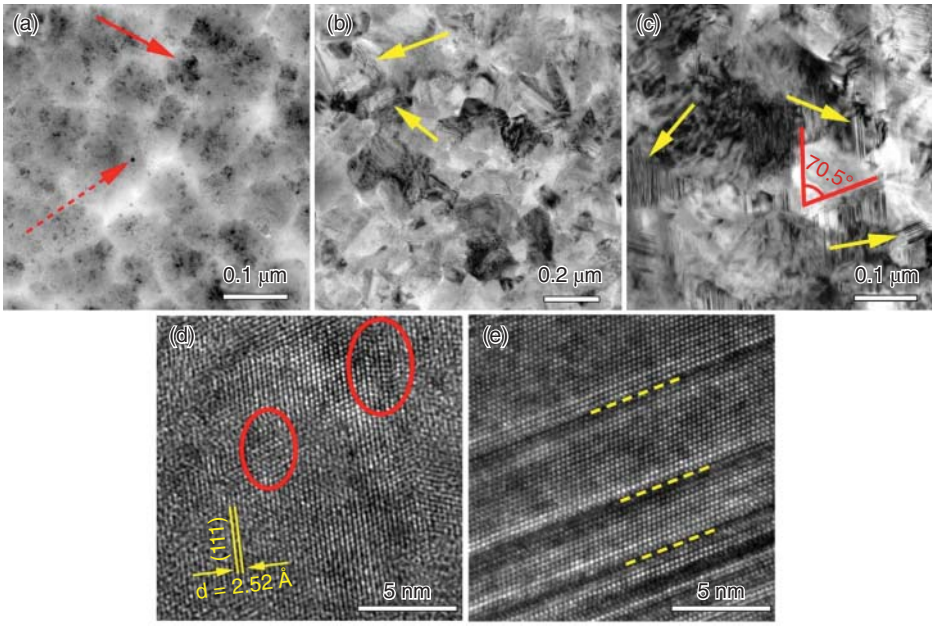


**Figure 1.3** Low magnification TEM images of a nanocrystalline (a), a microcrystalline (b), and an epitaxial (c) 3C-SiC film; HRTEM images of one typical 3C-SiC crystal in the nanocrystalline (d) and microcrystalline (e) 3C-SiC film. The arrows in (a) indicate the 3C-SiC crystals with different sizes in the nanocrystalline 3C-SiC film. The arrows in (b) and (c) indicate the existence of planar defects in the microcrystalline and epitaxial 3C-SiC films. The circles in (d) denote the existence of planar defects, of which positions are indicated with dashed lines in (e) [16]. Source: Reprinted with permission from ACS publisher, Copyright 2015.

planar defects (arrows) are also observed in the microcrystalline (Figure 1.3b) and epitaxial (Figure 1.3c) 3C-SiC films. Figure 1.3e shows the HRTEM image of one typical 3C-SiC microcrystal with planar defects indicated by the dashed lines. The formation of planar defects is difficult to avoid. It is a very common phenomenon during the growth of various SiC structures [56, 64]. This is because the formation energies of these planar defects are low. During MWCVD processes, the energy generated by the mismatches (e.g. lattice mismatch, thermal expansion coefficient mismatch, etc.) between the SiC film and the substrate is sufficient to trigger the formation of these phase defects, leading to their high concentration in the crystals. Even though the existence of the planar defects is clearly observable throughout the whole film, no small angle grain boundaries exist in the epitaxial 3C-SiC film. This indicates such an epitaxial 3C-SiC film can be viewed as a single 3C-SiC crystal but with a high density of planar defects. This result is in good accordance with the Raman observation, where the epitaxial 3C-SiC film is found to be composed solely of the 3C-SiC crystal without any amorphous phase.

Therefore, there are significant differences in the compositions of the nanocrystalline, microcrystalline, and epitaxial 3C-SiC films. Both nanocrystalline and microcrystalline 3C-SiC films consist of amorphous carbon, amorphous SiC, and 3C-SiC crystals, while the epitaxial 3C-SiC film is composed solely of 3C-SiC crystals. Moreover, there are big differences in the crystal sizes of the nanocrystalline and microcrystalline 3C-SiC films. Furthermore, both nanocrystalline and microcrystalline 3C-SiC films are polycrystalline, while the epitaxial 3C-SiC film shows perfect (001) orientation. In addition, a large number of planar defects are incorporated in the 3C-SiC crystals for the nanocrystalline, microcrystalline, and epitaxial 3C-SiC films [16].

### 1.3.2 Electrochemical Properties

Understanding the mechanisms of charge transfer across the interfaces of various SiC films and the electrolytes is of importance and significance. It is a basic prerequisite for exploring the practical applications of these SiC films [65].

SiC has been tried more than 70 years ago as an electrode. Single crystalline SiC film behaved in a similar way to a noble electrode [66]. Single SiC films were used to construct impedance and temperature sensors. SiC based biomedical needles were used for open-heart surgery monitoring and graft monitoring of organs during transportation and transplantation [67]. However, it was troublesome to get the right contacts due to low conductivities of these films. Later, the nanocrystalline 3C-SiC film was found to exhibit much higher electron mobility than a single crystalline SiC film [68, 69]. It was thus employed as a novel electrode material for electrochemical applications (e.g. for electrochemical sensing applications) [55, 70]. Moreover, the properties of 3C-SiC films, especially their electrochemical properties, were found to be tunable through controlling the microstructures of 3C-SiC films (e.g. crystallinity, crystal sizes, defects, and composition, etc.) [16]. For example, by manipulating the deposition conditions (e.g. power density, growth temperature, etc.) during MWCVD processes, the nanocrystalline, microcrystalline, and epitaxial (001) 3C-SiC films have been grown with altered electrochemical properties [16].

First, these 3C-SiC films exhibited different electrical conductivities, as measured by a four-point-probe technique. Both nanocrystalline and microcrystalline 3C-SiC films possess a sheet resistance of $\sim 3300\,\Omega\,\mathrm{cm}^{-2}$, whereas the epitaxial 3C-SiC film only